Environmental Science and Pollution Research (2022) 29:80109–80122
https://doi.org/10.1007/s11356-022-23394-x

REVIEW ARTICLE

Deformation failure and acoustic emission characteristics of continuous graded waste rock cemented backfill under uniaxial compression

Guan Chen[1] · Yicheng Ye[1,2] · Nan Yao[1] · Fanghui Fu[1] · Nanyan Hu[1] · Zhen Zhang[1]

Received: 5 May 2022 / Accepted: 27 September 2022 / Published online: 3 October 2022

Abstract

In order to study the effect of backfill aggregate particle size on the compressive strength and failure mode of cemented backfill, uniaxial compression tests were carried out on seven kinds of cemented backfills with different particle size gradations. By analyzing the AE characteristics during the failure process of the backfill, the damage evolution mechanism of the cemented backfill with different particle size gradations was discussed. The test results show that with the increase of the Talbot gradation index n, the compressive strength of the backfill specimens first increases and then decreases, and the failure mode gradually changes from shear failure to tensile failure. With the increase of particle size gradation, the particle size of aggregate increases, the interface between aggregate and cement matrix is more likely to be fractured, and the characteristic parameters of acoustic emission are more active. During the failure process of backfill, the AE energy rate increases rapidly in the plastic development stage, and reaches maximum value before and after the peak stress, which can be used as the precursor to judge the failure of waste rock cemented backfill. According to the test results, the damage model and constitutive equations of waste rock cemented backfill with different Talbot particle size gradations are established, which can provide engineering guidance for filling mined-out areas with waste rock to ensure safe production of mines.

Keywords Continuous gradation · Waste rock cemented backfill · Failure mode · Acoustic emission · Damage model

Introduction

During the mining of mineral resources, a large amount of solid waste (such as waste rock, tailings, and coal gangue) and goafs areas are generated (Li et al. 2019; Wang et al. 2022; Wu et al. 2021a; Yao et al. 2021). According to statistics, every 10,000 tons of ore mined will produce 9300 tons of tailings and 3400 tons of waste rock (Yan et al. 2022). With the increasing demand for mineral resources, the solid waste generated further increases. For example, the cumulative of solid waste has reached 60 billion tons in China by 2015, tailings and waste rock accounting for 14.6 billion tons and 43.8 billion tons (Sun et al. 2018). These solid wastes are usually stored in tailings ponds and storage yards, which is not only occupying a large amount of land resources, but also form an anthropogenic hazard source with high potential energy, which may lead to serious geotechnical accidents in extreme climates (Xin 2021). In addition, heavy metal ions such as copper ions, zinc ions, and lead ions in tailings will cause serious pollution to the mining environment (Behera et al. 2021; Chen et al. 2021b; Song et al. 2022; Xu et al. 2019).

With the increasing requirements of environmental protection, green mining strategies have been proposed, and the cemented tailings backfill mining method has become the most commonly used mining methods (Guo et al. 2022b; Wen et al. 2021; Yang et al. 2020; Zhang et al. 2022). Backfill mining is the preparation of tailings, cement, and water into a slurry at the surface, and then the slurry is transported to the underground goaf by gravity or pumping (Qiu et al. 2020b; Xin 2021). The hardened backfill can support the goaf areas, reduce surface subsidence, provide a safe

Responsible Editor: Philippe Garrigues

✉ Nan Yao
yaonan@wust.edu.cn

[1] School of Resources and Environmental Engineering, Wuhan University of Science and Technology, Wuhan 430081, China

[2] Industrial Safety Engineering Technology Research Center of Hubei Province, Wuhan 430081, China

operating environment, and can also turn waste into treasure, solve the problem of discharge and storage of solid waste in mining areas, reduce environmental pollution caused by mining of mineral resources and the cost of backfill mining (Behera et al. 2021; Bull and Fall 2020; Dong et al. 2019; Mahboub El et al. 2022).

As the key unit of backfill mining, the backfill plays an important role in maintaining the stability of the stope, especially the strength and failure law of the backfill are crucial to the effect of the backfill. The strength and mechanical properties of the backfill are closely related to the backfill material, cementitious material, lime-sand ratio, curing conditions, and other factors (Guo et al. 2022a; Li et al. 2021a; Meng et al. 2019; Wu et al. 2021b). At present, some scholars have carried out relevant research on the strength of cement tailings backfill. Qiu et al. (2020a) conducted uniaxial compression tests on cemented tailings backfills with different cement-sand ratios and waste rock content, the mechanical stability and failure modes are analyzed, and discussed the effects of cement-sand ratio and waste rock content on the mechanical stability of backfill specimens. Gao et al. (2019) used the RSM-BBD response surface method to study the effects of slurry mass fraction, mortar ratio and mixed aggregate ratio on strength, and determined the optimal mix ratio of mixed aggregate cemented backfill. Wu et al. (2022) studied the effect of carbon nanotube dosage and aggregate particle size distribution on mechanical properties and microstructure of cemented backfill. The results show that the microstructure of cemented rockfill with superior aggregate particle size distribution is uniform and dense, which is beneficial to the reinforcement of carbon nanotubes. Wang et al. (2020b) analyzed the strength variation law and failure characteristics of mixed consolidated of three kinds of density grade matrix through macroscopic mechanical test and microstructure observation, and the influence mechanism of gangue on the matrix strength was clarified.

AE technology is one of the most effective nondestructive testing techniques for predicting material instability and structural failure (Dzaye et al. 2020; Makhnenko et al. 2020; Zhou et al. 2021a). During the loading process, the damage evolution of the material's internal structure can be detected in real time, without causing additional damage to the material, which is helpful to deepening the understanding of material damage and destruction (Assi et al. 2018; Kocáb et al. 2019; Ma and Du 2020; Song et al. 2021). Therefore, it has been widely used in related engineering fields in recent years. Wang et al. (2020a) studied the mechanical behavior, failure mode, and damage evolution characteristics of different cement tailings ratios and layered cemented backfills with different structural characteristics. Zhou et al. (2021b) studied the damage evolution process and AE aging mechanism of tantalum-niobium tailings cemented backfill under uniaxial compression, and established a backfill damage model. Zhao et al. (2020) analyzed the mechanical properties and AE characteristics of tailings cemented backfill with different mass concentrations in uniaxial compression tests, determined the corresponding relationship between AE characteristics of failure precursors, and the change of slurry concentration. He et al. (2021) studied the failure law of cement slurry backfill and rock combination under pressure, and the tailings content has a significant effect on the crack evolution and AE characteristics of backfill at different stages.

The above studies show that the slurry mass concentration, lime-sand ratio, and structural characteristics have a great influence on the strength and failure form of the backfill. The cemented waste rock backfill is a paste-like backfill material, and there are few studies on the strength and failure laws of the waste rock backfill with different particle size gradations. Based on this, studying the effect of waste rock particle size grading on the mechanical strength and failure characteristics of the backfill, which can optimize the particle size grading of the waste rock backfill, improve the mechanical properties and stability of the backfill, and is of great significance to the safe mining of mines. In this work, the strength and failure characteristics of cemented backfills with different grades of waste rock were studied by uniaxial compression tests, and the dynamic evolution law of internal damage of backfills was revealed by AE characteristic parameters. Based on the Lemaitre strain equivalence principle, damage constitutive model was established, and its applicability and rationality were verified. The research results can provide a certain reference value for the waste rock cemented backfill to fill the goafs areas and ensure underground safe production.

Materials and methods

Experiment material

The waste rock used in the experiment was taken from Yichang, China. It is the block waste rock produced during the underground production development and recovery process of phosphate mines, and was crushed by the jaw crusher to coarse aggregate with a maximum particle size of 12 mm. The chemical composition of waste rock is shown in Table 1. The content of toxic and harmful elements is low, and it does not affect the underground environment and workers' health when used in underground goaf filling. In addition, the waste rock contains abundant CaO and MgO, which can provide sufficient strength support for the aggregate. The cementing material is 32.5 M Portland cement, which was widely applied in China. Table 1 gives its chemical composition, contained abundant SiO_2 (23.81%) and CaO (55.40%), which can provide sufficient strength and stability.

Table 1 Chemical compositions of waste rock and cement (%)

Materials	SiO_2	CaO	MgO	Al_2O_3	Fe_2O_3	K_2O	P_2O_5	SO_3	F	Others
Phosphate waste rock	7.53	54.85	19.91	1.39	1.20	1.95	10.32	1.03	0.39	1.43
Cement	23.81	55.40	2.50	6.79	3.25	1.14	-	3.87	-	3.24

Sample preparation

The particle size range of the coarse aggregate has a significant effect on the properties of cemented backfill, and the American Society for Testing and Materials (ASTM) (ASTM Standard C192/C192M-13a. 2013) recommends that the minimum diameter of cylindrical specimen must be at least 3 times the maximum particle size to eliminate size effects. Therefore, standard cylindrical specimen with diameter of 50 mm and height of 100 mm was prepared by using waste rock with a maximum particle size of 12 mm as filling aggregate, and 32.5 M Portland cement as cementing material.

The broken waste rock samples were sieved into 0–2, 2–4, 4–6, 6–8, 8–10, and 10–12 mm (as shown in Fig. 1), and the masses of the particles in these six intervals were Y_1, Y_2, Y_3, Y_4, Y_5, Y_6. In order to obtain the best filling effect, it was necessary to test different cemented backfill specimens made from different aggregate particles with a mass ratio of Y_1:Y_2:Y_3:Y_4:Y_5:Y_6, in the 6-dimensional space (Y_1:Y_2:Y_3:Y_4:Y_5:Y_6) to seek the optimal values of the peak strength, elastic modulus and deformation modulus of the cemented filling. The Talbot gradation theory was used to determine the mass ratio of waste rock in 6 particle size ranges, and the search space was reduced from 6 dimensions to 1 dimension to overcome the curse of dimensionality (Chen et al. 2021a; Wu et al. 2018; Wu et al. 2017). Assuming that the maximum particle size of the particles is x_{max}, according to Talbot gradation theory, the ratio of aggregate mass M with the particle size smaller than or equal to x in the sample to the total mass Mt of the aggregate particles is:

$$\frac{M}{M_t} = \left(\frac{x}{x_{max}}\right)^n \tag{1}$$

where n is the Talbot index.

According to Eq. (1), the mass of particles in the interval $[x_1, x_2]$ can be calculated as:

$$M_1^2 = \left[\left(\frac{x_2}{x_{\max}}\right)^n - \left(\frac{x_1}{x_{\max}}\right)^n\right] M_t \tag{2}$$

Table 2 shows the distribution of aggregate particles in waste rock cemented backfills under different Talbot gradation indices.

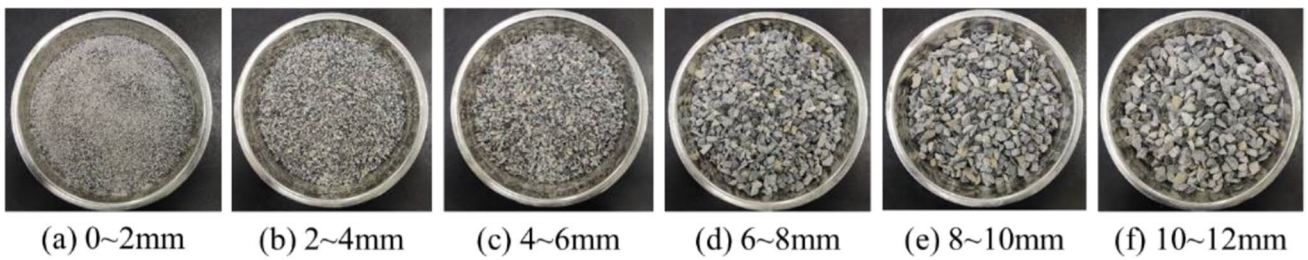

Fig. 1 Waste rock of different grain sizes

Table 2 Distribution of aggregate particles under different Talbot indexes

n	Mass percent (%) of particles in different size intervals (mm)					
	0–2	2–4	4–6	6–8	8–10	10–12
0.2	69.88	10.39	6.78	5.16	4.21	3.58
0.3	58.42	13.50	9.30	7.32	6.13	5.32
0.4	48.84	15.60	11.35	9.24	7.94	7.03
0.5	40.82	16.91	12.98	10.94	9.64	8.71
0.6	34.13	17.60	14.25	12.43	11.23	10.36
0.7	28.53	17.82	15.21	13.73	12.73	11.98
0.8	23.85	17.67	15.91	14.86	14.13	13.57

The fluidity of filling slurry is closely related to its transportation performance and work efficiency. When the mass concentration of the slurry is too high, segregation and stratification are likely to occur during the transportation of the slurry containing coarse particles, and the initial setting and final setting time of the slurry are prolonged, which seriously affects the engineering application of cemented backfill, and deteriorates the mechanical and structural properties of the backfill (Zuo et al. 2018). Therefore, based on the previous exploratory test, the lime-sand ratio to 1:6 and the slurry mass concentration to 86% was designed in this study. The detailed experimental scheme is shown in Table 3. According to the designed material ratio, the waste rock particles and cementing materials of different Talbot gradations were weighed, in turn, added quantitative water after, then mixed them evenly, and pour the evenly stirred slurry into the cylindrical mold three times. After the initial setting of the slurry, smooth the surface of the specimens, demolded the mold after standing for 48 h, and put it into a standard curing box with a temperature (20±2°C) and a humidity (95±2%) for curing. When the curing age reached 28 days, the specimens were taken out for uniaxial compression test.

Table 3 Experimental programs

Talbot index	Cement (g)	Waste rock (g)	Water (g)	Slump value (mm)
0.2	66.67	400	71.9	152
0.3	66.67	400	71.9	168
0.4	66.67	400	71.9	183
0.5	66.67	400	71.9	192
0.6	66.67	400	71.9	199
0.7	66.67	400	71.9	204
0.8	66.67	400	71.9	208

Experimental equipment and process

The YZM-30A microcomputer-controlled direct shearing instrument was used for the loading test, and the Express-8 AE acquisition system was used for the AE monitoring (as shown in Fig. 2). After the samples reached the curing age, they were subjected to uniaxial compression tests. Before the loading test, choose the undamaged sample, grind both ends of it flat, and the fine particles on the surface were removed. The stress loading mode was used to slowly load to 0.1 kN, and then the displacement loading mode was used to load the sample to failure, and the loading rate was 0.002 mm/s (Wang et al. 2021b). A total of 4 probes are used in the experiment, 2

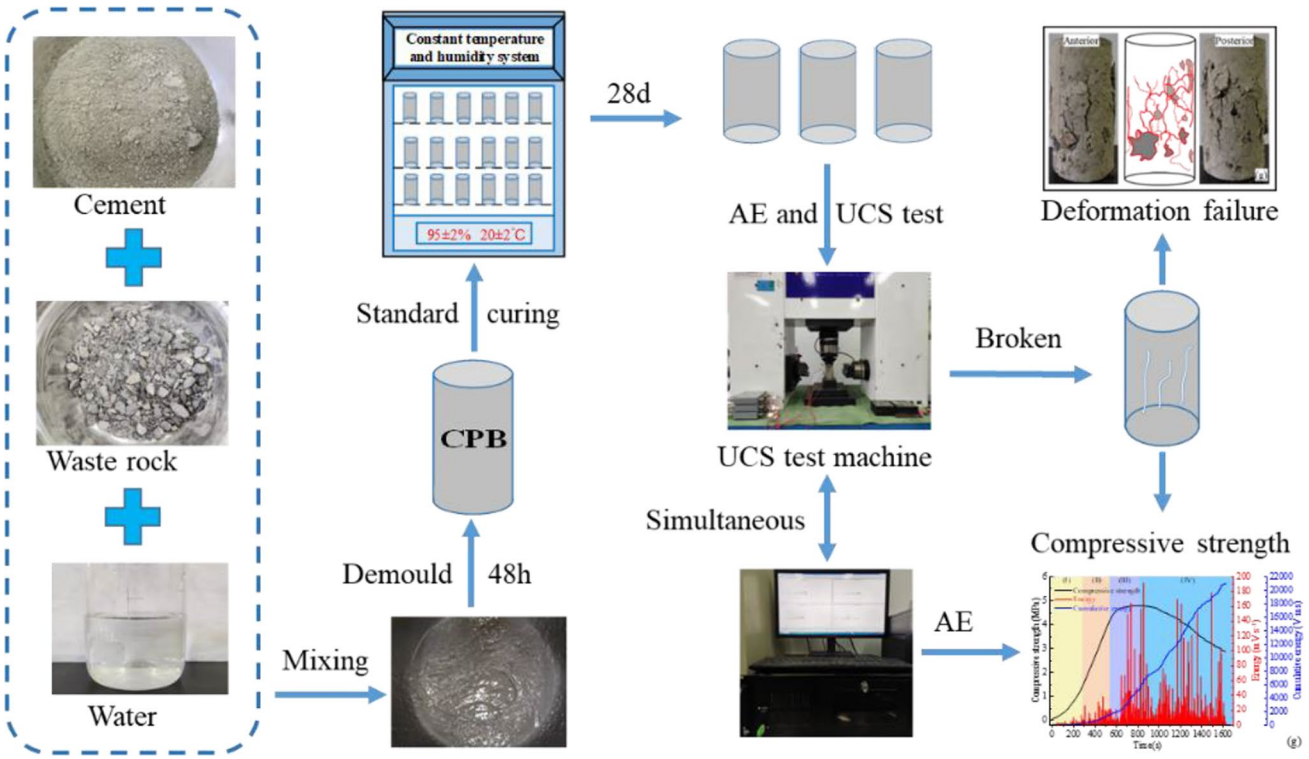

Fig. 2 Experimental procedure

at the upper and 2 at the lower ends of the specimens. The AE test system and its probes spatial positioning map are shown in Fig. 3, which was set with the preamplifier gain which is 40 dB, waveform threshold is 40 dB, sampling rate is 100 kHz–10 MHz, and the sampling frequency is 3 MHz. During the test, Vaseline was applied to the contact area between the probe and the backfill specimens to ensure coupling contact with the sample surface. The operations of AE and loading equipment are carried out at the same time to ensure the correspondence of data time nodes.

Result and discussion

Uniaxial compressive strength

The uniaxial compressive strengths of different grades of waste rock cemented backfills are shown in Fig. 4. With the increase of Talbot particle size gradation index n, the compressive strength of cemented backfill showed a trend of first increasing and then decreasing. When the gradation index n is less than 0.4, as the gradation index n increases, the particle size of waste rock particles increases, which reduces the specific surface area of solid material in the backfill, increases the cement content per unit area, the cementation effect is better, and the compressive strength of the backfill is higher. When the gradation index n is greater than 0.4, with the increase of the gradation index n, the fine particles in the backfill specimens decrease, and the pores between the coarse particles cannot be filled completely. In addition, when the proportion of coarse particles is large, the cement cannot completely encapsulate them, resulting in the weakening of cementation effect in the backfill, and the compressive strength of waste rock cemented backfill gradually decreases.

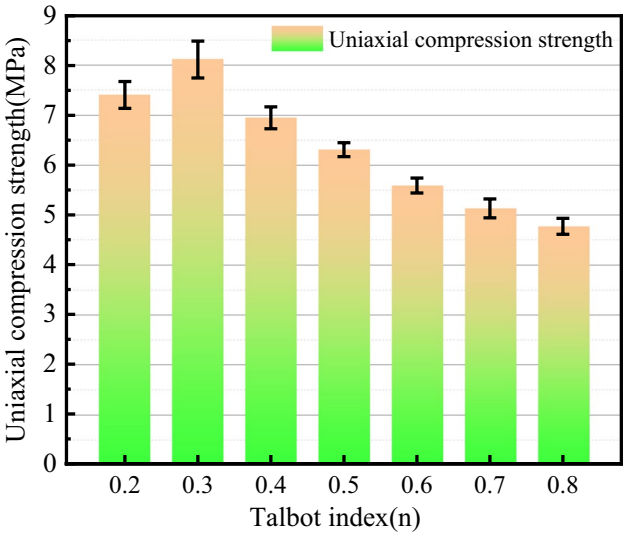

Fig. 4 Strength characteristics of cemented backfill body

Destruction feature mode of backfill

The typical failure morphology of waste rock cemented backfills with different Talbot particle size gradations under uniaxial compression is shown in Fig. 5. (The left and right pictures show the final failure state of the specimen, and the middle is the sketch of cracks.) When the Talbot gradation index n is 0.2, 0.3, and 0.4, the content of coarse aggregate in backfill specimens is less, and the boundary transition area between aggregate and cementitious matrix is larger. Under the loading, the cracks inside backfill specimen are initiated from the stress concentration at the sharp corners of aggregate, develop along the boundary of fine aggregate and then penetrate through the structure, and the failure mode is semi-penetrating truncation failure. When the Talbot gradation index n is 0.5, and 0.6, the content of coarse aggregate in backfill specimen increases, and the transition area between aggregate and cementitious matrix decreases. Under the loading, the interface between coarse aggregate

Fig. 3 AE test system and its probe spatial positioning map

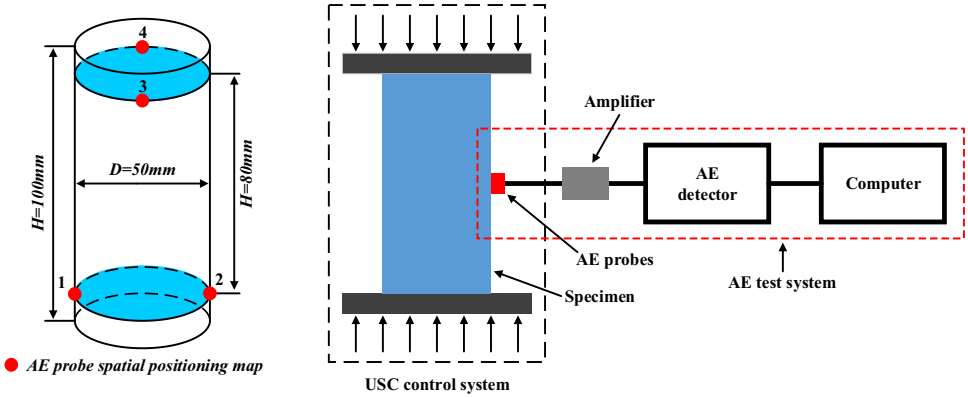

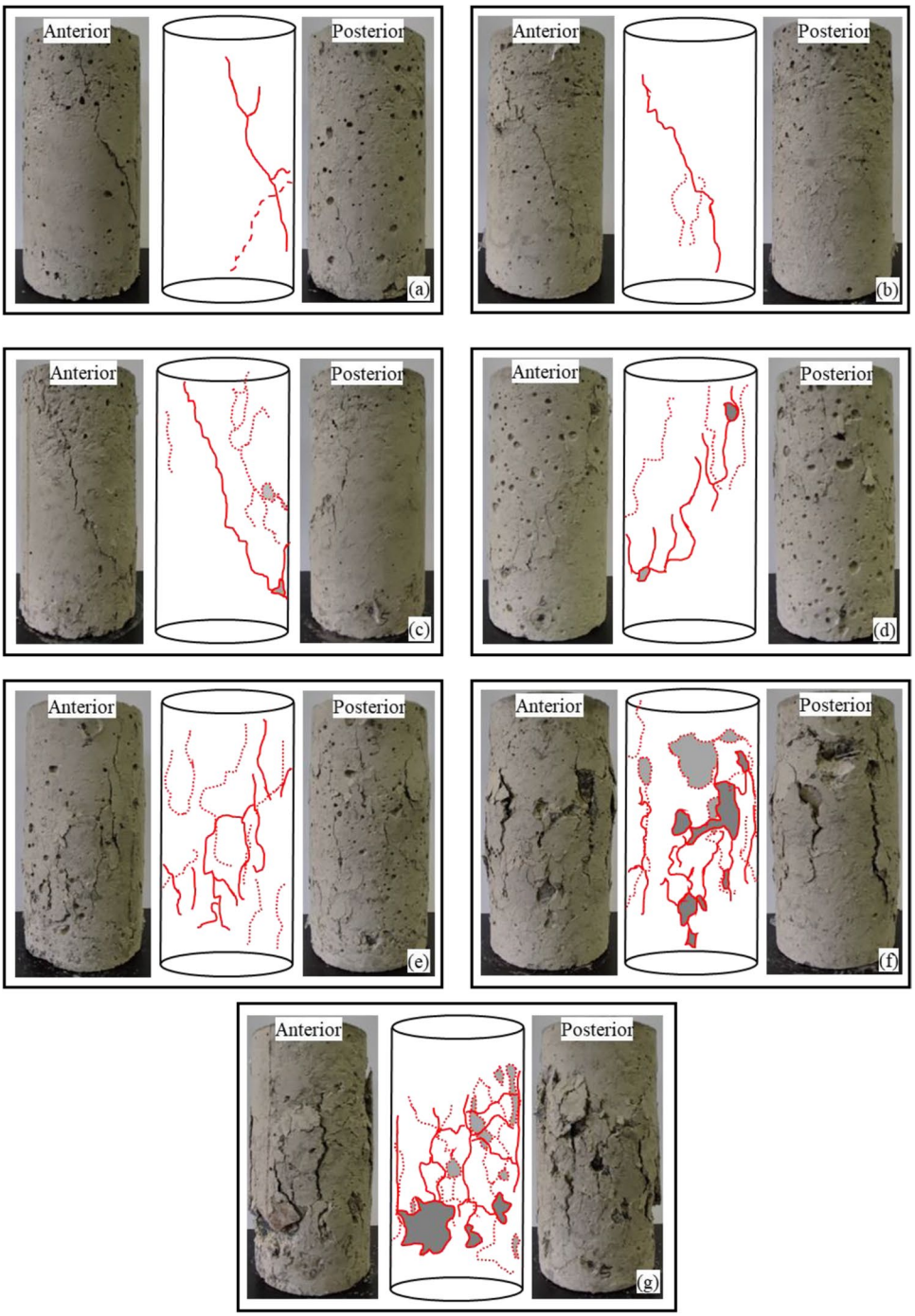

Fig. 5 Failure modes of cemented backfill with different mix ratios. (**a**) n=0.2; (**b**) n=0.3; (**c**) n=0.4; (**d**) n=0.5; (**e**) n=0.6; (**f**) n=0.7; (**g**) n=0.8

and cementitious matrix fractures, local cracks accumulated, and the failure mode of backfill specimen gradually changes from shear failure to tensile failure. When the Talbot gradation index n was 0.7, and 0.8, the content of coarse aggregate particles in backfill specimens is higher, which further strengthened the friction effect between coarse aggregate particles. Under the loading, the interface between coarse aggregate and cementitious matrix fractures and slips, the coarse aggregate particles rub and squeeze each other. The accumulation of local stress causes different degrees of fragmentation in the middle area of the backfill specimen, and the failure mode is tensile failure parallel to the loading direction.

By analyzing the failure characteristics of the waste rock cemented backfill specimens, it is known that under uniaxial loading, the original cracks inside the waste rock cemented backfill expand and connect to form macroscopic cracks, which eventually lead to the failure of backfill. The

distribution characteristics of coarse aggregate particles have a significant effect on the uniaxial compressive strength and deformation failure characteristics of the cemented backfill (Yin et al. 2021). When the Talbot gradation index n is small, the failure form of backfill specimens is shear failure, and there are fewer cracks on the specimen surface. With the increase of the Talbot gradation index n, the failure form of backfill specimens gradually changed from shear failure to tensile failure, the number of cracks associated with the surface of specimens gradually increased, and the surface was accompanied by more block exfoliation, the damage is more serious.

Acoustic emission characteristics

Numerous studies have shown that AE is a concomitant phenomenon of releasing strain energy externally in the form of elastic wave in the process of fracture development and expansion. The AE signals during the loading process can reflect the evolution law of internal fracture expansion (Guo et al. 2021). During the damage and destruction of backfill specimen, the development and expansion of the internal fissures have obvious stages, and the corresponding AE signals have certain differences. Figure 6 shows the AE signals of waste rock cemented backfill with different Talbot particle size gradations during the deformation and failure process. The waste rock cemented backfill specimens can be divided into four stages under uniaxial compression process: I-pore compaction stage, II-elastic deformation stage, III-plastic development stage, and IV-destruction stage (Hou et al. 2021; Li et al. 2021b; Zhao et al. 2022).

In the pore compaction stage (I) and elastic deformation stage (II), the primary pores in backfill specimen are gradually compacted, and the AE energy rate is at a low level. In the plastic development stage (III), with the increase of external load, the interface between aggregate and cementitious matrix begins to fracture, forming new cracks. Strain energy is released during crack initiation and development, so the AE energy rate increases rapidly and reaches a maximum value before and after the peak stress. Therefore, the rapid increase in the AE energy rate can be regarded as a precursor to the failure of cemented waste rock backfill. In the failure stage (IV), the rapid development of micro-cracks gradually evolved into macro-cracks visible to the naked eye, the damage degree of backfill specimen increased, and the AE energy rate remained at a high level for a long time.

It can be seen from Fig. 6(a)–(g) that with the gradual increase of the Talbot particle size gradation index n, the AE energy rate and the cumulative energy rate gradually increase. This is due to the increase of Talbot gradation index n, the content of coarse aggregate in backfill specimen increases. Under the loading, the coarse aggregate particles squeeze each other, resulting in an increase in the fracture area of interface between aggregate particles and the cementitious matrix, and the AE energy rate is also higher (Qiu et al. 2022).

Spatial evolution of acoustic emission event points

The spatial evolution of AE event points of waste rock cemented backfill specimens with different Talbot particle size gradations during uniaxial compression is shown in Fig. 7. The "sphere" in the figure is the AE event point. By analyzing the changes of the spatial position, volume size, number, and color of the "sphere" volume, the position, size, number, and corresponding time of the cracks in the backfill specimen can be reflected. It can be seen from Fig. 7 that with the increase of Talbot particle size gradation index n, the content of coarse aggregate particles gradually increases, and the number and volume of AE event points gradually increase. This is because the interface between coarse aggregate and cementitious matrix is fractured under the loading, and the coarse aggregate rubs and squeezes each other, which further aggravates the damage of the backfill sample.

Figure 8 shows the proportion of AE energy ratios of waste rock cemented backfills with different Talbot particle size gradations in different loading stages. It can be seen from Fig. 8 that with the increase of Talbot particle size gradation index n, the proportion of AE energy rate of backfill specimen gradually decreases in pore compaction stage and elastic deformation stage, and increases in failure stage. Due to the increase of particle size gradation index n, the proportion of coarse aggregate particles increases, and the fine aggregate and cementitious matrix cannot completely fill the pores between skeletons, resulting in the increase of primary pores in the backfill specimen. In the pore compaction stage and elastic deformation stage, when the particle size gradation index is larger, there are more pores in the specimen, fewer microcracks are generated under loading, and the proportion of AE energy rate is lower. Therefore, in pore compaction stage, the proportion of AE energy rate gradually decreased from 13.83 to 1.03%, in elastic deformation stage, it gradually decreased from 18.66 to 6.22%. In failure stage, when the particle size gradation index n is larger, the fracture area of interface between aggregate particles and cementitious matrix is larger, the number of cracks produced is more, and the proportion of AE energy rate is higher. Thereby, in destruction stage, the proportion of AE energy gradually increased from 42.68 to 74.99%.

Damage model and constitutive equation of waste rock cemented backfill

The waste rock cemented backfill specimen is regarded as an isotropic continuous medium, and the damage is a continuous process under the action of external load. According to

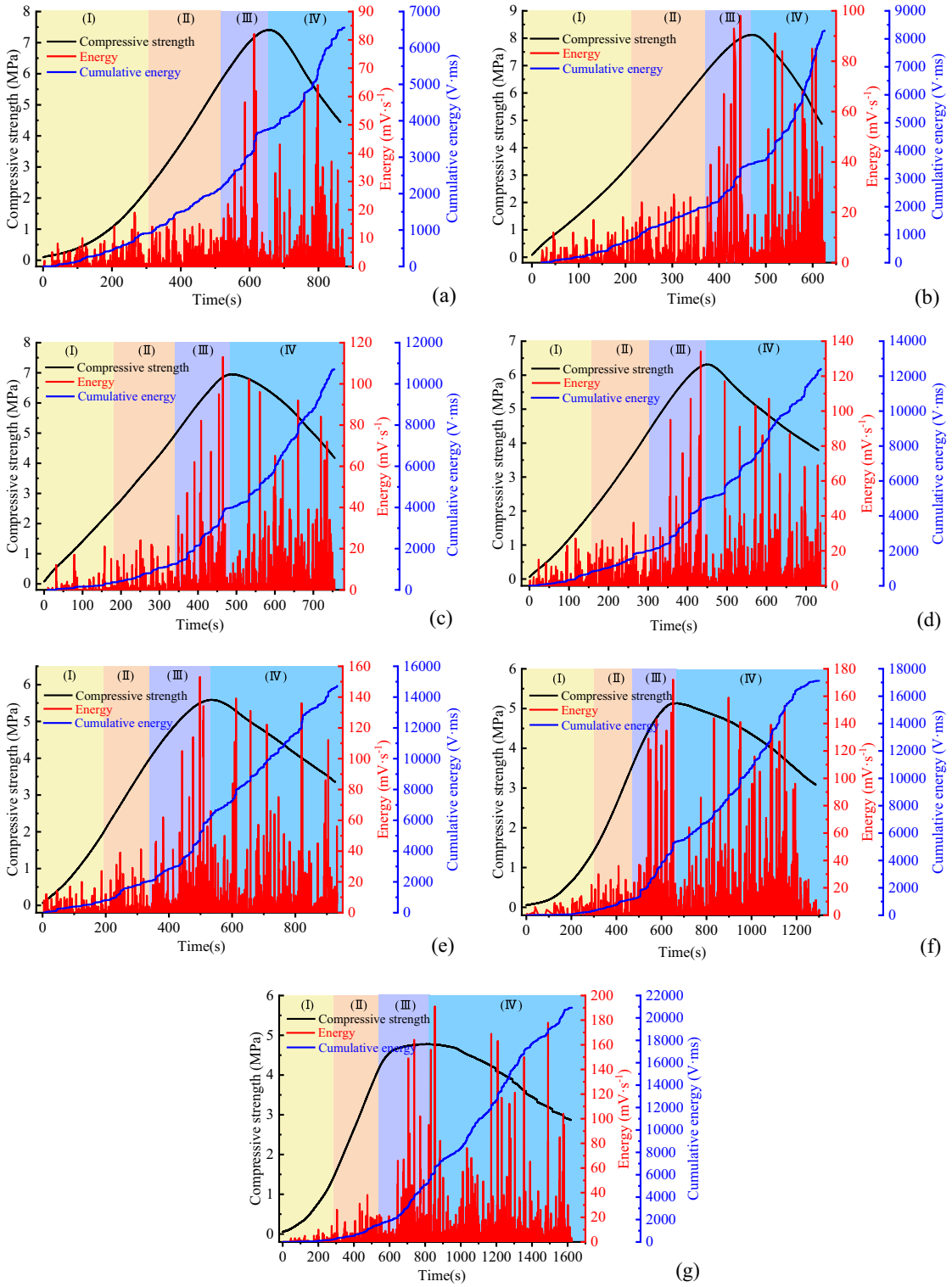

Fig. 6 AE energy, cumulative energy and stress-time curve of cemented backfill. (**a**) n=0.2; (**b**) n=0.3; (**c**) n=0.4; (**d**) n=0.5; (**e**) n=0.6; (**f**) n=0.7; (**g**) n=0.8

the Lemaitre strain equivalence principle (Liu et al. 2018; Wang et al. 2020a; Wang et al. 2019; Zhao et al. 2019), the damage stress of the filling body under uniaxial compression can be defined as Eq. (3).

$$\sigma = E\varepsilon(1 - D) \tag{3}$$

In Eq. (3): σ is the effective stress of the backfill; E is the elastic modulus of the backfill; ε is the strain value of

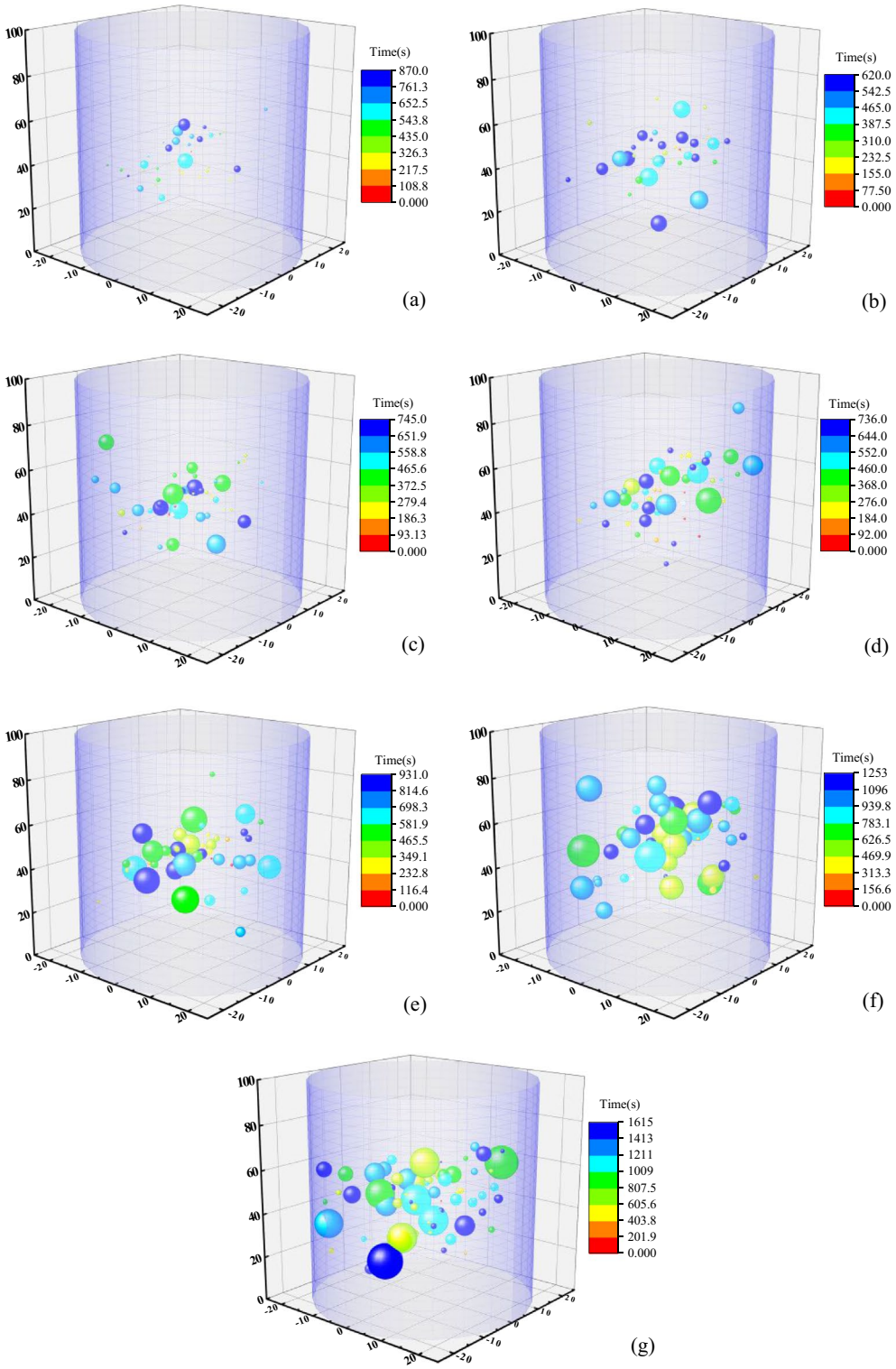

Fig. 7 Spatial evolution of AE event points of backfill body specimens over time. (**a**) n=0.2; (**b**) n=0.3; (**c**) n=0.4; (**d**) n=0.5; (**e**) n=0.6; (**f**) n=0.7; (**g**) n=0.8

the backfill; D is the damage factor of the backfill. When $D = 0$, the backfill is in a non-damaged state; When $D = 1$, the backfill is completely destroyed.

According to the characteristics of the stress-strain relationship curve after the failure of the filling sample, it can be described by the density function of the Weibull statistical

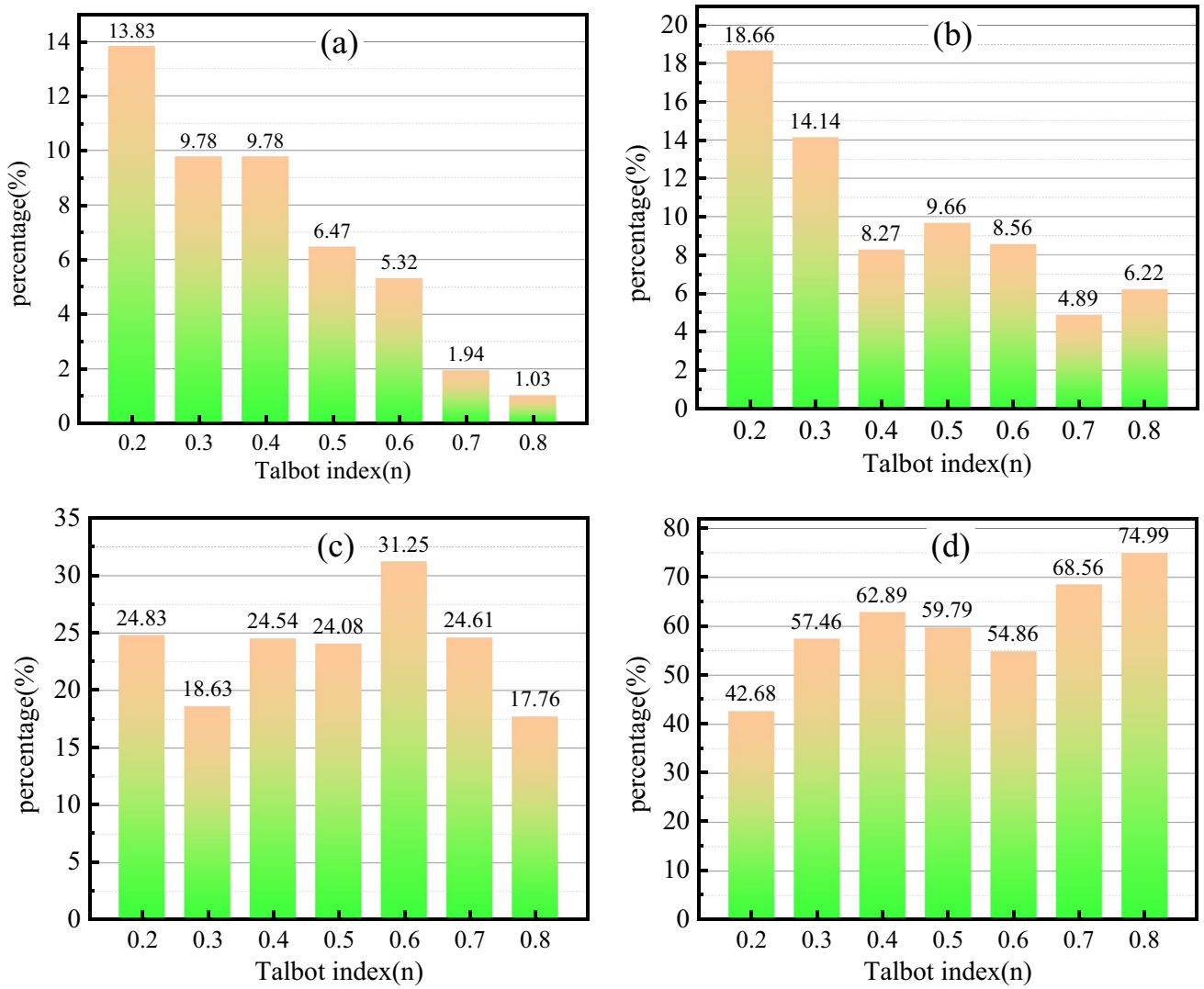

Fig. 8 Proportion of AE energy rate of waste rock cemented backfill in different failure stages. (**a**) pore compaction stage; (**b**) elastic deformation stage; (**c**) plastic development stage; (**d**) destruction stage

distribution (Wang et al. 2018). Since the strength σ of the backfill obeys the Weibull distribution, combined with the relationship between D and σ in Eq. (3), the damage variable D of the backfill also obeys the Weibull distribution, and the relationship between the damage variable and the strain is derived as in Eq. (4):

$$D = 1 - \exp\left[-\frac{1}{k}\left(\frac{\varepsilon}{\varepsilon_p}\right)^{|k|}\right] \tag{4}$$

Substituting Eq. (4) into Eq. (3), the damage constitutive equation of the backfill specimens can be obtained, such as Eq. (5).

$$\sigma = E\varepsilon \exp\left[-\frac{1}{k}\left(\frac{\varepsilon}{\varepsilon_p}\right)^{|k|}\right] \tag{5}$$

In Eq. (5), ε_p is the peak strain; k is a parameter related to material properties.

The calculation formula of k value is as Eq. (6):

$$k = \frac{1}{\ln\left(\frac{E\varepsilon_p}{\sigma_p}\right)} \tag{6}$$

According to the stress-strain relationship curve obtained by the uniaxial compression test of the backfill specimens, the elastic modulus E, property parameters k and $1/k$ were calculated, and the damage constitutive equation of waste rock cemented backfill with different Talbot particle size gradations was obtained, as shown in Table 4.

According to the damage constitutive equation of waste rock cemented backfill with different Talbot

Table 4 Damage constitutive equation for cemented backfill of waste rock with different particle size gradation

Talbot index	Damage stress equation σ	Damage evolution equation D
0.2	$\sigma=817.32\varepsilon\exp[-0.37(\varepsilon/0.0131)^{2.72}]$	$D=1-\exp[-0.37(\varepsilon/0.0131)^{2.72}]$
0.3	$\sigma=1097.65\varepsilon\exp[-0.24(\varepsilon/0.0094)^{4.16}]$	$D=1-\exp[-0.24(\varepsilon/0.0094)^{4.16}]$
0.4	$\sigma=887.09\varepsilon\exp[-0.21(\varepsilon/0.0097)^{4.68}]$	$D=1-\exp[-0.21(\varepsilon/0.0097)^{4.68}]$
0.5	$\sigma=930.19\varepsilon\exp[-0.29(\varepsilon/0.0091)^{3.41}]$	$D=1-\exp[-0.29(\varepsilon/0.0091)^{3.41}]$
0.6	$\sigma=709.52\varepsilon\exp[-0.32(\varepsilon/0.0108)^{3.17}]$	$D=1-\exp[-0.32(\varepsilon/0.0108)^{3.17}]$
0.7	$\sigma=727.18\varepsilon\exp[-0.64(\varepsilon/0.0134)^{1.56}]$	$D=1-\exp[-0.64(\varepsilon/0.0134)^{1.56}]$
0.8	$\sigma=529.64\varepsilon\exp[-0.6(\varepsilon/0.0164)^{1.68}]$	$D=1-\exp[-0.6(\varepsilon/0.0164)^{1.68}]$

particle size grading in Table 4, the comparison between theoretical and experimental curves of waste rock cemented backfill with different particle size gradation is obtained, as shown in Fig. 9. The development trend of the theoretical curve of backfill specimen is the same as that of the experimental curve, and the overall agreement is good. Due to the existence of pores compaction stage, elastic deformation stage, and yield stage in the loading process of backfill specimen, it is difficult for theoretical formula to simulate the real situation of different loading stages at the same time (Wang et al. 2021a). But in general, the theoretical curve is in good agreement with the experimental curve, which can objectively characterize the uniaxial compression process of cemented waste rock backfill.

By analyzing the theoretical damage curve of backfill specimens, it is known that the damage variable is closely related to the deformation characteristics of backfill. The damage curves of cemented backfill with Talbot graded waste rock all show an increasing trend of "S". When the peak strain of backfill specimen is small (as shown in Fig. 9(b), (c), (d), and (e)), the curve of damage variable is more obvious before the peak stress, the damage variable increases slowly, and the damage variable that corresponds to the peak stress is small ($D < 0.3$). In contrast, when the peak strain is large (as shown in Fig. 9(f), and (g)), the damage variable curve does not bend significantly before the peak stress, the damage variable increases rapidly, and the damage variable corresponding to the peak stress is higher ($D > 0.4$). After the peak stress, due to the strong plasticity of backfill specimen, the bearing capacity decreases slowly, and the damage variable increases slowly.

Conclusions

In this paper, waste rock cemented backfill samples with different Talbot particle size gradations were designed and obtained, and then the mechanical properties and damage evolution law of backfill were studied by uniaxial AE emission test. Finally, the damage constitutive model of cemented backfill of waste rock with different particle size gradations is established, and the main conclusions are as follows:

(1) With the increase of Talbot particle size gradation index n, the compressive strength of backfill first increased and then decreased. When the particle size gradation index n increases, the particle size of waste rock increases, which reduces the specific surface area of aggregate in the backfill, increases the amount of hydration products per unit area, and improves the compressive strength of the backfill. When the content of coarse aggregate is too large, the fine particles are not enough to completely encapsulate the coarse aggregate, which leads to the weakening of cementation effect between the coarse aggregates and reduces the compressive strength of the backfill.

(2) With the increase of Talbot particle size gradation index n, the internal structure of backfill specimen changed. When the particle size gradation index n is 0.2, 0.3, and 0.4, the crack develops along the weak part of interface between cementation matrix and aggregate, finally penetrates the backfill specimen, and the failure mode of backfill is shear failure. As the gradation index n increases, the proportion of coarse aggregate increases, the coarse aggregates squeeze each other, cracks accumulate in the middle area of the specimen, and the failure mode gradually changes from shear failure to tensile failure.

(3) During the loading process, with the increase of the particle size gradation index n, the AE energy rate and the cumulative energy rate both increased. In pore compaction stage and elastic deformation stage, the AE rate is at a low value. With the increase of external load, the AE energy increases rapidly and reaches the maximum value at the peak stress, which can be used as a precursor of backfill failure.

(4) By comparing the theoretical curve and experimental curve, the overall agreement between the two is good, indicating that the established damage constitutive model of the cemented waste rock backfill is reliable and has certain guiding significance for engineering applications.

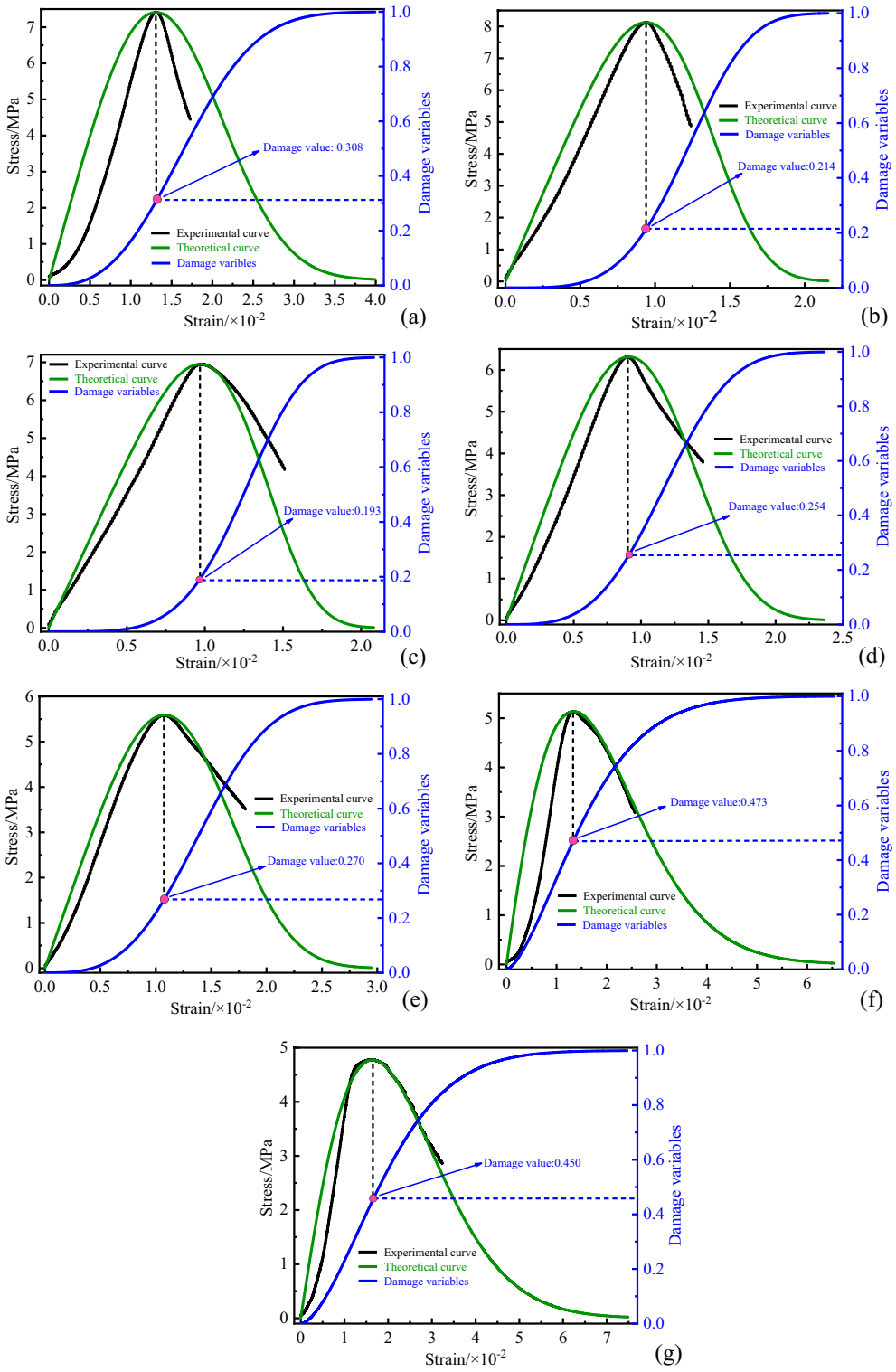

Fig. 9 Stress-strain test and theoretical curve of backfill body specimens. (a) n=0.2; (**b**) n=0.3; (**c**) n=0.4; (**d**) n=0.5; (**e**) n=0.6; (**f**) n=0.7; (**g**) n=0.8

Author contribution Guan Chen and Nan Yao conceived and designed the experiments. Yicheng Ye guided the experiment and the writing of the thesis. Guan Chen, Fang Hui Fu, and Zhen Zhang performed the experiments. Guan Chen and Nan Yan Hu analyzed the data. All authors contributed to the writing of the manuscript and approved the final manuscript.

Funding This work is supported by the Key Research and Development Plan of Hubei Province (No. 2020BCA082), National Natural Science Foundation of China (No. 51804224), Wuhan University of Science and Technology 2021 Graduate Innovation and Entrepreneurship Fund Project (No. JCX2021139).

Data availability The datasets used and/or analyzed during the current study are available from the corresponding author on reasonable request.

Declarations

Competing interests The authors declare no competing interests.

References

Assi L, Soltangharaei V, Anay R, Ziehl P, Matta F (2018) Unsupervised and supervised pattern recognition of acoustic emission signals during early hydration of Portland cement paste. Cem Concr Res 103:216–225. https://doi.org/10.1016/j.cemconres.2017.10.019

ASTM Standard C192/C192M-13a (2013) Standard practice for making and curing concrete test specimens in the lab. Annual Book of ASTM Standards, West Conshohocken, PA. Available online:. https://doi.org/10.1520/C0192_C0192M-13A.

Behera SK, Mishra DP, Prashant S, Mishra K, Mandal SK, Ghosh CN, Ritesh K, Mandal PK (2021) Utilization of mill tailings, fly ash and slag as mine paste backfill material: review and future perspective. Constr Build Mater 309:125120. https://doi.org/10.1016/j.conbuildmat.2021.125120

Bull AJ, Fall M (2020) Curing temperature dependency of the release of arsenic from cemented paste backfill made with Portland cement. J Environ Manag 269:110772. https://doi.org/10.1016/j.jenvman.2020.110772

Chen AP, Dong FS, Shu PF, Fu ZX (2021a) Mechanical properties and acoustic emission characteristics of continuous graded cemented backfill. J Huazhong Univ Sci Tech 49(08):46–52. https://doi.org/10.13245/j.hust.210809

Chen G, Ye YC, Yao N, Hu NY, Zhang J, Huang Y (2021b) A critical review of prevention, treatment, reuse, and resource recovery from acid mine drainage. J Clean Prod 329:129666. https://doi.org/10.1016/j.jclepro.2021.129666

Dong LJ, Tong XJ, Li XB, Zhou J, Wang SF, Liu B (2019) Some developments and new insights of environmental problems and deep mining strategy for cleaner production in mines. J Clean Prod 210:1562–1578. https://doi.org/10.1016/j.jclepro.2018.10.291

Dzaye ED, De Schutter G, Aggelis DG (2020) Monitoring early-age acoustic emission of cement paste and fly ash paste. Cem Concr Res 129:105964. https://doi.org/10.1016/j.cemconres.2019.105964

Gao Q, Yang XB, Wen ZJ, Chen DX, He JY (2019) Optimization of proportioning of mixed aggregate filling slurry based on BBD response surface method. J Hunan Univ 46(6): 47-55. 10.16339/j.cnki.hdxbzkb.2019.06.007

Guo LZ, Zhou M, Wang XY, Li C, Jia HQ (2022a) Preparation of coal gangue-slag-fly ash geopolymer grouting materials. Constr Build Mater 328:126997. https://doi.org/10.1016/j.conbuildmat.2022.126997

Guo YX, Ran HY, Feng GR, Du XJ, Zhao YH, Xie WS (2022b) Deformation and instability properties of cemented gangue backfill column under step-by-step load in constructional backfill mining. Environ Sci Pollut Res Int 29:2325–2341. https://doi.org/10.1007/s11356-021-15638-z

Guo YX, Zhao YH, Feng GR, Ran HY, Zhang YJ (2021) Study on damage size effect of cemented gangue backfill body under uniaxial compression. Chin J Rock Mech Eng 40(12):2434–2444. https://doi.org/10.13722/j.cnki.jrme.2021.0527

He ZW, Zhao K, Yan YJ, Ning FJ, Zhou Y, Song YF (2021) Mechanical response and acoustic emission characteristics of cement paste backfill and rock combination. Constr Build Mater 288:123119. https://doi.org/10.1016/j.conbuildmat.2021.123119

Hou YQ, Yin SH, Chen X, Zhang MZ, Yang SX (2021) Study on characteristic stress and energy damage evolution mechanism of cemented tailings backfill under uniaxial compression. Constr Build Mater 301:124333. https://doi.org/10.1016/j.conbuildmat.2021.124333

Kocáb D, Topolář L, Kucharczyková B, Halamová R (2019) The analysis of acoustic emission signals detected during the loading of cement-based materials. Eng Fail Anal 99:18–25. https://doi.org/10.1016/j.engfailanal.2019.01.002

Li JJ, Erol Y, Cao S (2021a) Influence of industrial solid waste as filling material on mechanical and microstructural characteristics of cementitious backfills. Constr Build Mater 299:124288. https://doi.org/10.1016/j.conbuildmat.2021.124288

Li M, Zhang JX, Wj S, Germain DM (2019) Recycling of crushed waste rock as backfilling material in coal mine: effects of particle size on compaction behaviours. Environ Sci Pollut Res Int 26(9):8789–8797. https://doi.org/10.1007/s11356-019-04379-9

Li ZF, Zhang C, Zhang J, Jin Q, Wang YS, Yan N (2021b) Mechanical properties and damage mechanism of backfill with different water saturation. J Min Safe Eng 38(05): 1063-1069+107. 10.13545/j.cnki.jmse.2020.0383

Liu XS, Tan YL, Ning JG, Lu YW, Gu QH (2018) Mechanical properties and damage constitutive model of coal in coal-rock combined body. Int J Rock Mech Min 110:140–150. https://doi.org/10.1016/j.ijrmms.2018.07.020

Ma GF, Du QJ (2020) Structural health evaluation of the prestressed concrete using advanced acoustic emission (AE) parameters. Constr Build Mater 250:118860. https://doi.org/10.1016/j.conbuildmat.2020.118860

Mahboub El K, Mbonimpa M, Belem T, Maqsoud A (2022) Rheological characterization of cemented paste backfills containing superabsorbent polymers (SAPs). Constr Build Mater 317:125863. https://doi.org/10.1016/j.conbuildmat.2021.125863

Makhnenko RY, Ge CW, Labuz Joseph F (2020) Localization of deformation in fluid-saturated sandstone. Int J Rock Mech Min 134:104455. https://doi.org/10.1016/j.ijrmms.2020.104455

Meng GH, Li M, Wu ZY, Ma HB, Wang YY (2019) The effects of high temperature on the compaction behaviour of waste rock backfill materials in deep coal mines. B Eng Geol Environ 79(2):845–855. https://doi.org/10.1007/s10064-019-01603-1

Qiu HF, Zhang FS, Liu L, Hou DZ, Tu BB, Zhao YL (2020a, 2020) Influencing factors on strength of waste rock tailing cemented backfill. Geofluids:1–7. https://doi.org/10.1155/2020/8847623

Qiu HF, Zhang FS, Liu L, Huan C, Hou DZ, Kang W (2022) Experimental study on acoustic emission characteristics of cemented rock-tailings backfill. Constr Build Mater 315:125278. https://doi.org/10.1016/j.conbuildmat.2021.125278

Qiu JP, Guo ZB, Yang L, Jiang HQ, Zhao YL (2020b) Effects of packing density and water film thickness on the fluidity behaviour of cemented paste backfill. Powder Technol 359:27–35. https://doi.org/10.1016/j.powtec.2019.10.046

Song HQ, Zuo JP, Liu HY, Zuo SH (2021) The strength characteristics and progressive failure mechanism of soft rock-coal combination samples with consideration given to interface effects. Int J Rock Mech Min 138:104593. https://doi.org/10.1016/j.ijrmms.2020.104593

Song XP, Hao YX, Wang S, Zhang L, Liu HB, Yong FW, Dong ZL, Yuan Q (2022) Dynamic mechanical response and damage evolution of cemented tailings backfill with alkalized rice straw under SHPB

cycle impact load. Constr Build Mater 327:127009. https://doi.org/10.1016/j.conbuildmat.2022.127009
Sun W, Wang HJ, Hou KP (2018) Control of waste rock-tailings paste backfill for active mining subsidence areas. J Clean Prod 171:567–579. https://doi.org/10.1016/j.jclepro.2017.09.253
Wang B, Wang F, Wang Q (2018) Damage constitutive models of concrete under the coupling action of freeze–thaw cycles and load based on Lemaitre assumption. Constr Build Mater 173:332. https://doi.org/10.1016/j.conbuildmat.2018.04.054
Wang J, Fu JX, Song WD, Zhang YF, Wang Y (2020a) Mechanical behavior, acoustic emission properties and damage evolution of cemented paste backfill considering structural feature. Constr Build Mater 261:119958. https://doi.org/10.1016/j.conbuildmat.2020.119958
Wang J, Song WD, Tan YY, Fu JX, Cao S (2019) Damage constitutive model and strength criterion of horizontal stratified cemented backfill. Rock Soil Mech 40(05):1731–1739. https://doi.org/10.16285/j.rsm.2018.0017
Wang J, Fu J, Song W, Zhang Y (2021a) Mechanical properties, damage evolution, and constitutive model of rock-encased backfill under uniaxial compression. Constr Build Mater 285:122898. https://doi.org/10.1016/j.conbuildmat.2021.122898
Wang WQ, Ye YC, Wang QH, Hu NY (2021b) Experimental study on anisotropy of strength, deformation and damage evolution of contact zone composite rock with DIC and AE techniques. Rock Mech Rock Eng 55(2):837–853. https://doi.org/10.1007/s00603-021-02682-x
Wang XF, Cao WH, Zhanng DS, Yang H, Chang ZC, Cai WY (2020b) Mechanism study on influence of particle size and content of gangue on strength of high-sand and high-foam cement-based filling material. J Min Safe Eng 37(02):376–384. https://doi.org/10.13545/j.cnki.jmse.2020.02.018
Wang ZQ, Wang Y, Cui L, Bi C, Wu AX (2022) Insight into the isothermal multiphysics processes in cemented paste backfill: effect of curing time and cement-to-tailings ratio. Constr Build Mater 325:126739. https://doi.org/10.1016/j.conbuildmat.2022.126739
Wen ZJ, Xiao BL, Gao Q, Yin SH, Wang Y (2021) Study on strength influencing factors and strength model of cemented backfill with mixed aggregate. Arab J Geosci 14(9). https://doi.org/10.1007/s12517-021-07175-3
Wu J, Jing H, Gao Y, Meng Q, Yin Q, Du Y (2022) Effects of carbon nanotube dosage and aggregate size distribution on mechanical property and microstructure of cemented rockfill. Cem Concr Compos 127:104408. https://doi.org/10.1016/j.cemconcomp.2022.104408
Wu JY, Feng MM, Mao XB, Xu JM, Zhang WL, Ni XY, Han GS (2018) Particle size distribution of aggregate effects on mechanical and structural properties of cemented rockfill: experiments and modeling. Constr Build Mater 193:295–311. https://doi.org/10.1016/j.conbuildmat.2018.10.208
Wu JY, Feng MM, Yu BY, Chen ZQ, Mao XB, Han GS (2017) Experimental study of strength and deformation characteristics of cemented waste rock backfills with continuous gradation. Rock Soil Mech 38(01):101–108. https://doi.org/10.16285/j.rsm.2017.01.013
Wu JY, Jing HW, Meng QB, Yin Q, Yu LY (2021a) Assessment of cemented waste rock backfill for recycling gangue and controlling strata: creep experiments and models. Environ Sci Pollut Res Int 28. https://doi.org/10.1007/s11356-021-12944-4
Wu JY, Yin Q, Gao Y, Meng B, Jing HW (2021b) Particle size distribution of aggregates effects on mesoscopic structural evolution of cemented waste rock backfill. Environ Sci Pollut Res Int 28(13):16589–16601. https://doi.org/10.1007/s11356-020-11779-9
Xin LW (2021) Meso-scale modeling of the influence of waste rock content on mechanical behavior of cemented tailings backfill. Constr Build Mater 307:124473. https://doi.org/10.1016/j.conbuildmat.2021.124473
Xu DM, Zhan CL, Liu HX, Lin HZ (2019) A critical review on environmental implications, recycling strategies, and ecological remediation for mine tailings. Environ Sci Pollut Res Int 26(35):35657–35669. https://doi.org/10.1007/s11356-019-06555-3
Yan ZP, Yin SH, Chen X, Wang LM (2022) Rheological properties and wall-slip behavior of cemented tailing-waste rock backfill (CTWB) paste. Constr Build Mater 324:126723. https://doi.org/10.1016/j.conbuildmat.2022.126723
Yang L, Xu WB, Erol Y, Wang Q, Qiu JP (2020) A combined experimental and numerical study on the triaxial and dynamic compression behavior of cemented tailings backfill. Eng Struct 219:110957. https://doi.org/10.1016/j.engstruct.2020.110957
Yao HH, Cai LB, L. Wei, Qing WQ, Jiao F, Yang CR (2021) Current status and development of comprehensive utilization of waste rock in metal mines in China. Chinese J Nonferrous Met 31(06): 1649-1660. https://doi.org/10.11817/j.ysxb.1004.0609.2021-35986
Yin SH, Hou YQ, Yang SX, Li MZ, Cao Y (2021) Analysis of deformation failure and energy dissipation of mixed aggregate cemented backfill during uniaxial compression. J Cent South Univ 52(03):936–947. https://doi.org/10.11817/j.issn.1672-7207.2021.03.025
Zhang MG, Li KQ, Ni W, Zhang SQ, Liu ZY, Wang K, Wei XL, Yu Y (2022) Preparation of mine backfilling from steel slag-based non-clinker combined with ultra-fine tailing. Constr Build Mater 320:126248. https://doi.org/10.1016/j.conbuildmat.2021.126248
Zhao K, Song YF, Yu X, Zhou Y, Yan YJ, Wang JQ (2022) Study on early mechanical properties and damage constitutive model of cemented tailings backfill under different fibers. Chin J Rock Mech Eng 41(02):282–291. https://doi.org/10.13722/j.cnki.jrme.2021.0369
Zhao K, Xie WJ, Zeng P, Gong C, Zhou YL, Yu XJ, Yang ZY, Liu ZC (2020) Experimental study on AE characteristics of cemented tailings backfill failure process with different concentration. J Appl Acoust 39(04):543–549. https://doi.org/10.11684/j.issn.1000-310X.2020.04.007
Zhao K, Zhu ST, Zhou KP, Yan YJ, Zhao K, Li Q, Gu SJ (2019) Research on mechanical properties and damage law of tantalum-niobium ore cemented tailings backfill. J Min Safe Eng 36(02):413–419. https://doi.org/10.13545/j.cnki.jmse.2019.02.026
Zhou Y, Yan YJ, Zhao K, Yu X, Song YF, Wang JQ, Suo TY (2021a) Study of the effect of loading modes on the acoustic emission fractal and damage characteristics of cemented paste backfill. Constr Build Mater 277:122311. https://doi.org/10.1016/j.conbuildmat.2021.122311
Zhou Y, Yu X, Guo ZQ, Yan YJ, Zhao K, Wang JQ, Zhu ST (2021b) On acoustic emission characteristics, initiation crack intensity, and damage evolution of cement-paste backfill under uniaxial compression. Constr Build Mater 269:121261. https://doi.org/10.1016/j.conbuildmat.2020.121261
Zuo JP, Hong ZJ, Xiong ZQ, Wang C, Song HQ (2018) Influence of different W/C on the performances and hydration progress of dual liquid high water backfilling material. Constr Build Mater 190:910–917. https://doi.org/10.1016/j.conbuildmat.2018.09.146